J. Membrane Biol. 169, 91–102 (1999)

The Journal of
Membrane
Biology

Quantitative Determination of Gap Junctional Permeability in the Lens Cortex

R. Eckert[1], B. Adams[2], J. Kistler[1], P. Donaldson[2]
[1]School of Biological Sciences and [2]School of Medicine, University of Auckland, Auckland, New Zealand

Received: 1 December 1998/Revised: 22 February 1999

Abstract. We have developed a simple dye transfer method, which allows the gap junction permeability of lens fiber cells to be quantified. Two fixable fluorescent dyes (Lucifer yellow and rhodamine-dextran) were introduced into peripheral lens fiber cells via mechanical damage induced by removing the lens capsule. After a defined incubation period, lenses were fixed, sectioned, and the distribution of the dye recorded using confocal microscopy. Rhodamine-dextran and Lucifer yellow both labeled the extracellular space between fiber cells and the cytoplasm of fiber cells that had been damaged by capsule removal. For the gap junctional permeable dye Lucifer yellow, however, labeling was not confined to the damaged cells and exhibited intercellular diffusion away from the damaged cells. The extent of dye diffusion was quantified by collecting radial dye intensity profiles from the confocal images. Effective diffusion coefficients (D_{eff}) for Lucifer yellow were then calculated by fitting the profiles to a series of model equations, which describe radial diffusion in a sphere. D_{eff} is the combination of dye diffusion through the cytoplasm and through gap junction channels. To calculate the gap junctional permeability (P_j) an estimate of the cytoplasmic diffusion coefficient ($D_{cyt} = 0.7 \times 10^{-6}$ cm^2/sec) was obtained by observing the time course of dye diffusion in isolated elongated fiber cells loaded with Lucifer yellow via a patch pipette. Using this approach, we have obtained a value for P_j of 31×10^{-5} cm/sec for fiber-fiber gap junctions. This value is significantly larger than the value of P_j of 4.4×10^{-6} cm/sec reported by Rae and coworkers for epithelial-fiber junctions (Rae et al., 1996. *J. Membrane Biol.* **150:**89–103), and most likely reflects the high abundance of gap junctions between lens fiber cells.

Correspondence to: P. Donaldson

Key words: Lens — Intercellular communication — Dye transfer — Gap junctions — Diffusion modeling

Introduction

Traditionally, intracellular injection of fluorescent dyes has been used to establish whether cells can communicate via gap junction channels (Loewenstein, 1981). Dye injection is a relatively easy method to perform and has been used to estimate a molecular cutoff for gap junction channel pore size (Flagg-Newton, Simpson & Loewenstein, 1979). More recently, the development of the highly sensitive double whole-cell patch-clamp technique (Neyton & Trautmann, 1985; Veenstra & DeHaan, 1986) has allowed measurements of single channel conductances and voltage sensitivities for different isoforms of the gap junction proteins, the connexins (Werner, 1998). These electrical properties provide a useful fingerprint for the identification of distinct connexin isoforms in different tissues but it is now widely considered that the permeability properties of connexins are more important for tissue function, especially in the case of nonexcitable cells. Unfortunately, while it has been shown that different connexin isoforms exhibit differential permselectivities (Elfgang et al., 1995; Brink, 1996; Veenstra, 1996), data on absolute permeability values for gap junctional membranes are scarce. Hence, there is a growing interest in systems where gap junction permeability can be quantified.

The ocular lens presents itself as a suitable system. The bulk of the lens consists of highly differentiated elongated fiber cells that are tightly packed in a quasi-crystalline arrangement (Rafferty, 1985) and are extensively coupled by gap junctions (Donaldson et al., 1995; Mathias, Rae & Baldo, 1997). The cortical fiber cells are particularly rich in gap junction structures which contain two connexins, connexin46 (α3) and con-

nexin50 (α8) (Kistler, Christie & Bullivant, 1988; Paul et al., 1991; White et al., 1992) which are both essential for the normal function of the lens (Gong et al., 1997; White, Goodenough & Paul, 1998). This is due to the fact that the lens is an avascular tissue and, therefore, relies on intercellular communication via gap junctions to provide a pathway for nutrient uptake and waste product removal.

This abundance of gap junctions connecting the fiber cells and their highly regular arrangement make the lens an ideal tissue to study gap junctional permeability with fluorescent tracers. Indeed, injection of tracer dyes into single fiber cells of the lens has been used to demonstrate intercellular communication (Schuetze & Goodenough, 1982; Prescott et al., 1994). This approach cannot, however, be used to quantitate junctional permeability since the microelectrode delivers inadequate amounts of dye relative to the large volume of the injected fiber cell. The amount of tracer that can pass into neighboring cells is, therefore, very low and specialized imaging equipment and analysis procedures have to be employed to raise the fluorescence signal above the signal-to-noise ratio (Rae et al., 1996). As an alternative solution to avoid the technical problems associated with microinjection we have developed a simple bulk loading method for measuring intercellular dye transfer in the lens. Our method is an adaptation of the scrape-loading technique successfully used to visualize dye transfer in cell monolayers (el-Fouly, Trosko & Chang, 1987). This method uses two fixable fluorescent dyes of different molecular weight as markers for cell loading and diffusion through gap junctions. The high molecular weight dye rhodamine-dextran (MW 10,000) is impermeable through gap junctions and, therefore, identifies the cells that have initially been loaded with tracer. The low molecular weight dye Lucifer yellow (MW 457) is gap junction permeable and acts as a tracer for diffusion through gap junction channels. Both dyes are loaded into the lens by mechanical damage inflicted by removal of the lens capsule. By fitting appropriate diffusion models to the intensity distribution of the Lucifer yellow fluorescence, we were then able to determine a value for the absolute permeability of the gap junctions that connect the fiber cells in the lens cortex.

Materials and Methods

Isolation of Lens Fiber Cell Bundles

Rat lens fiber cell bundles were isolated as previously described (Eckert, Donaldson & Kistler, 1998). Briefly, 3–5-day-old neonate Wistar rats were killed by decapitation and the eyes were removed. Eyeballs were placed in a Ca^{2+}-free Ringer's solution (in mM): 147 NaCl, 4.7 KCl, 2 $MgCl_2$, 5 glucose, 10 HEPES, pH 7.4, and the lenses extracted through a posterior opening. Following incubation in Ca^{2+}-free Ringer for 30 min, the lenses were further dissected and the capsule and the lens nucleus were removed using sharpened forceps. The cortical fiber cell portions of six lenses were pooled in an Eppendorf tube with 500 μL of dissociation solution (SEH in mM): 280 sucrose, 10 Na_2EDTA, 10 HEPES, and 2.5 mg/mL trypsin, pH 7.4, and incubated for 25 min at 37°C. The trypsin reaction was stopped by addition of an equal volume of newborn calf serum and the cells were spun down at 1,000 rpm and resuspended in 1 mL EDTA-Ringer's solution (in mM): 100 NaCl, 4.7 KCl, 1 $MgCl_2$, 25 glucose, 60 mannitol, 10 EDTA, 10 HEPES, pH 7.4). The cell suspension was washed with EDTA-Ringer's, resuspended in a final volume of 500 μL EDTA-Ringer's saturated with halothane and maintained at 37°C.

Dye Diffusion in Isolated Fiber Cell Bundles

For intracellular dye diffusion measurements, isolated fiber cell bundles were spread on the glass bottom of a recording chamber and left to adhere for 5 to 10 min before filling the chamber with EDTA-Ringer's solution. The chamber was then placed onto the stage of an inverted microscope (IM35, Zeiss, Oberkochen, Germany) equipped with phase contrast and epifluorescence optics. Patch pipettes were pulled from borosilicate glass capillaries (Clark Biomedical, Pangbourne, UK) to a final resistance of 2–5 MΩ using a Brown-Flaming type horizontal pipette puller (P-97, Sutter Instrument) and backfilled with a 0.5% (w/v) Lucifer yellow CH in lithium chloride pipette solution (in mM): 140 LiCl, $MgCl_2$, 10 K_2EGTA, 10 HEPES, pH 7.4). Standard whole-cell recording techniques (Marty & Neher, 1983) were used to perfuse a single fiber cell of a bundle with the dye solution.

To prevent loss of dye into the neighboring cells, fiber cells were kept in EDTA Ringer's solution saturated with halothane for about 10 min before initiating the experiments. A series of 15 fluorescence images were captured at 10-sec intervals with a cooled CCD camera (ImagePoint, Photometrics) and the image acquisition program V (Digital Optics, Auckland, New Zealand). The first image of a sequence was always taken before membrane break-in to obtain a well defined starting point for the time series. No iontophoretic current was used in these experiments.

Whole Lens Dye Loading Protocols

Wistar rats (200–350 g) were killed by CO_2 asphyxiation and the lenses were extracted from the eye. Lenses were placed in phosphate buffered saline (Ca^{2+}/Mg^{2+} free PBS (in mM): 137 NaCl, 2.7 KCl, 9.2 Na_2HPO_4, 1.2 KH_2PO_4, pH 7.3), and maintained at room temperature. For whole lens dye transfer studies the capsule and the underlying epithelium were removed. Lenses were placed under a dissecting microscope, and a small tear was made in the posterior surface of the capsule. Specially sharpened forceps were used to peel off the capsule from the lens. Each lens was then transferred to an individual well molded from sylgard, which was filled with 60 μL of tracer dye solution (2.5 mg/mL of rhodamine conjugated dextran and Lucifer yellow in Ca^{2+}/Mg^{2+} free PBS). After dye loading for the specified times (5, 10, 20, or 30 min), lenses were rapidly washed in 2 mL of Ca^{2+}/Mg^{2+} free PBS, and then immediately fixed in 25% Karnovsky's solution (0.05 M Na cacodylate, 1% paraformaldehyde, 1.25% glutaraldehyde) in PBS for 4 h. Intracellular pH was lowered by preincubating lenses in Ca^{2+}/Mg^{2+} free PBS saturated with 100% CO_2 (pH = 6.3) for 10 min before incubation in dye loading solution, which was also presaturated with 100% CO_2. Halothane was administered by preincubating lenses in a PBS solution for 10 min which was continually bubbled (flow rate 1 L/min) with a mixture of 5% halothane and 95% O_2 as a

carrier gas. Dye loading was performed in the continued presence of halothane for a further 10 min before fixation.

Lens Sectioning and Confocal Microscopy

Fixed lenses were superglued to a Vibratome holder and embedded in 10% agarose for added stability. Equatorial sections were cut with a thickness of 200 μm using a Vibratome. Sections were mounted on glass microscope slides and dye distribution was visualized by confocal microscopy. Only equatorial sections, which exhibited the flat hexagonal cross-profile characteristic of fiber cells, were used for analysis of radial dye diffusion in the lens. Specimens were viewed using a Leica TCS 4D confocal laser-scanning microscope fitted with an argon/krypton mixed gas laser. Either a 5× dry 0.12 N.A., 25× oil, 0.75 N.A. or 63× oil, 1.4 N.A. objective lens was used. Appropriate filter sets were used to discriminate between the Lucifer yellow (Ex488/OG515) and rhodamine-dextran (Ex568/OG590) light emissions. Initially, the pinhole and photomultiplier tube voltage settings of the confocal microscope were varied to determine optimal levels for minimal slice thickness, resolution, and dye intensity. In subsequent experiments a constant pinhole was used and the photomultiplier voltage was varied so that the image collected utilized the full dynamic range of the imaging system. All images were collected separately and stored on the hard disk until further processing.

Image Analysis and Quantification of Dye Diffusion

Stored images were analyzed offline using UTSCSA ImageTool 2.0α. To estimate cytoplasmic dye diffusion in single fiber cells, consecutive images of a time sequence were ordered into an image stack. Intensity profiles were then taken along the length of the perfused fiber cell for all images in the time sequence. The profiles were then stored as a text file for further analysis. To estimate radial dye diffusion in whole lenses, Lucifer yellow and rhodamine-dextran images collected from an equatorial section were aligned and overlaid into an image stack. In each of these images, intensity profiles were taken through the cytoplasm of a column of fiber cells at a direction perpendicular to the broad sides of the fiber cells. This was done to minimize the contribution of extracellular dye to the intensity profile. Rhodamine-dextran intensity profiles were used to define the extent of the dye-loading zone. From each set of images, five intensity profiles were taken from different regions where the loading zone for rhodamine-dextran was sharply defined. These intensity profiles were averaged and then saved as text files for further analysis. All profiles were scaled to their correct length using the built-in spatial calibration facility of UTSCSA ImageTool.

Diffusion Profile Analysis

At low concentration of the fluorescent dye fluorescence intensity is linearly related to dye concentration (Taylor & Salmon, 1989). For Lucifer yellow fluorescence quenching, which would abolish this linear relationship, occurs only at concentrations above 2 mM (Brink & Ramanan, 1985). The expected cytoplasmic dye concentration after fixation is well below this threshold, therefore, the Lucifer yellow intensity profiles can be directly used to measure the extent of dye diffusion that occurs prior to lens fixation. Intensity profiles for individual lenses were imported into the graphics package Microcal Origin 4.1. Profile data were normalized and the mean and standard deviation of the intensity profile for each lens calculated. Model equations as detailed in the theory section below were then fitted to the calculated mean intensity profiles to estimate the effective diffusion coefficient D_{eff} for radial dye transfer or D_{cyt} for cytoplasmic diffusion. The presence of background fluorescence was accounted for either by background subtraction, or by the introduction of a constant offset term into the formulae used for curve fitting. Diffusion coefficients were entered into the statistical analysis package SPSS for Windows 6.1.3. The data were grouped into treatment groups and tested for normal distribution using the Kolmogorov-Smirnov Goodness of Fit test. Mean diffusion coefficients and standard deviations were calculated for each group. ANOVA was used to determine whether treatment groups were significantly different at the $P < 0.05$ level.

Modeling of Diffusion Profiles in the Lens

To model radial diffusion in the whole lens and longitudinal diffusion in an isolated fiber cell we have used the spreadsheet program (Microsoft Excel) to implement the finite difference solution of the diffusion equation (Press et al., 1992) as described in the Appendix. Due to the limitation of the spreadsheet solution only the explicit Foreward Time Centered Space (FTCS) differencing scheme was used, which is only stable for small time increments $\Delta t < (\Delta x)^2/(2D)$. MS-Excel spreadsheets containing the time evolution of the tracer concentration were directly imported into the graphics program (Origin 4.1) and subjected to the same fitting procedures as the respective experimental data.

Theory

Tracer Diffusion in Whole Lenses

For the derivation of analytical solutions of the diffusion equation for dye concentration profiles in the lens we assume that the lens is an ideal sphere, which is surrounded by a large volume of dye, so that during the course of the dye loading the concentration of dye in the exterior space does not change. Initially, the lens contains no intrinsic dye, so background fluorescence will be minimal and constant within the total volume of the lens. Thus we can write the diffusion equation for spherical coordinates

$$\frac{\partial C}{\partial t} = \frac{1}{r^2}\left(\frac{\partial}{\partial r}\left(Dr^2\frac{\partial C}{\partial r}\right) + \frac{1}{\sin\theta}\frac{\partial}{\partial \theta}\left(D\sin\theta\frac{\partial C}{\partial \theta}\right) + \frac{D}{\sin^2\theta}\frac{\partial^2 C}{\partial \phi^2}\right) \quad \text{(Eq. 1)}$$

Neglecting transport in angular direction, this becomes

$$\frac{\partial C}{\partial t} = D\left(\frac{\partial^2 C}{\partial r^2} + \frac{2}{r}\frac{\partial C}{\partial r}\right) \quad \text{(Eq. 2)}$$

For large radius of the lens r (flat curvature at the lens surface), the second term becomes negligible, and the problem reduces to the conventional one-dimensional diffusion problem

$$\frac{\partial C}{\partial t} = D\frac{\partial^2 C}{\partial r^2}. \quad \text{(Eq. 3)}$$

which can be solved analytically for a number of initial and boundary conditions. Specifically, we were interested in solutions for two distinct scenarios. The first scenario assumes that the dye is constantly supplied from the periphery of the lens, that is

$$C(0,t) = C_0 \mid t > 0 \quad \text{(Eq. 4)}$$

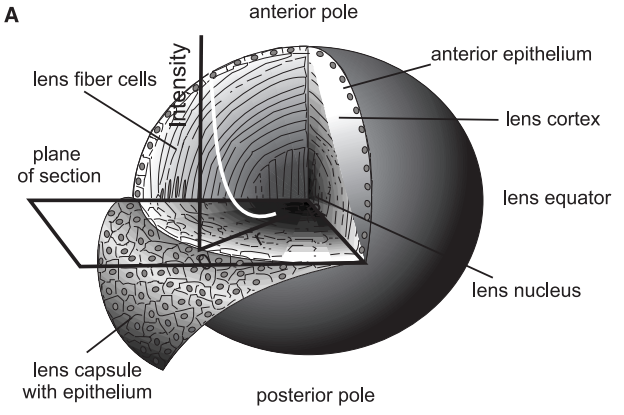

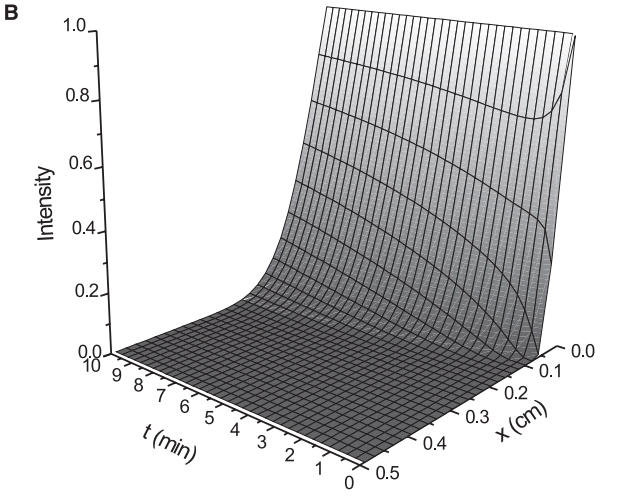

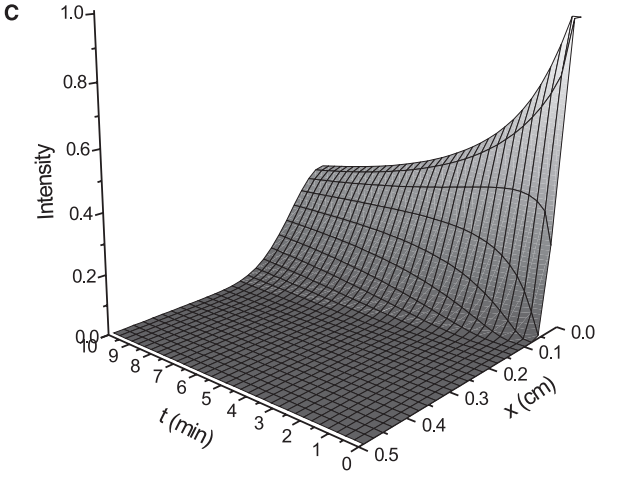

Fig. 1. Modeling of gap junction tracer diffusion in the lens. (*A*) Geometry of the rat lens. The equatorial sections used in the study produce cross-sectional profiles of the fiber cells (*see* plane of section). The lens capsule and the anterior epithelium is removed during the dye loading procedure. Note, that the radial coordinate x for the intensity profiles is running from the periphery ($x = 0$) to center of the lens ($x = R$). Typical diameters for lenses used in this study are around 5 mm. (*B*) Tracer distribution for continuous loading from the periphery assuming a constant tracer concentration in the surrounding medium. (*C*) Tracer distribution for discontinuous loading from the periphery (bolus loading). This model assumes that the peripheral fiber cell membranes regain their integrity such that only a fixed amount of tracer is incorporated into the cytoplasmic compartment. The profile sequences shown represent the first 10 min of the time course for lenses with a diameter of 4 mm. For clarity only the outer 500 μm representing the outer cortex are shown.

This has the solution (Crank, 1975)

$$C(x,t) = C_0 \operatorname{erfc} \frac{x}{2\sqrt{Dt}} \qquad \text{(Eq. 5)}$$

Note, that we have changed the spatial variable to x, which now runs in opposite direction with $x = 0$ denoting the outer border of the lens, and $x = R$ at lens center (*see* Fig. 1*A*). A simulation of the time course for the intensity distribution of a tracer dye through the peripheral part of the lens is shown in Fig. 1*B*.

The second scenario assumes that a finite amount of dye M_0 is initially distributed within the lens at a boundary layer of width h, and then allowed to diffuse inwards

$$C(x,t) = \frac{1}{2} C_0 \left(\operatorname{erf}\left(\frac{(h-x)}{2\sqrt{Dt}} \right) + \operatorname{erf}\left(\frac{(h+x)}{2\sqrt{Dt}} \right) \right). \qquad \text{(Eq. 6)}$$

This also assumes, that the border at $x = 0$ is a reflective boundary

$$\frac{\partial C}{\partial x} = 0 \qquad \begin{vmatrix} x = 0 \\ t \geq 0 \end{vmatrix}, \qquad \text{(Eq. 7)}$$

that is, loading occurs in a bolus fashion after which the outer surface "reseals" and the dye is trapped within the lens volume. Note, that this also implies that

$$\int_0^R C dx = M_0 \quad | t \geq 0 \qquad \text{(Eq. 8)}$$

i.e., the total amount of tracer does not change over time. This can be seen in a model simulation (Fig. 1*C*), where the maximum concentration (intensity) decreases over time as the dye distribution widens. Note the typical sigmoidal shape of the distribution at longer diffusion times. In contrast, for continuous loading, the distribution maintains the maximal intensity level at the boundary, and the shape of the profile is notably different. The model simulations show the tracer distribution in the outer 500 μm of a spherical lens with 4 mm diameter.

In both models, D is the effective diffusion coefficient for the combination of dye diffusion through the cytoplasm and permeation through gap junction channels. This effective diffusion coefficient D_{eff} can be related to gap junctional permeability P_j via (Ramanan & Brink, 1990)

$$\frac{1}{D_{eff}} = \frac{1}{D_{cyt}} + \frac{1}{d_{fiber} P_j} \qquad \text{(Eq. 9)}$$

Thus, given the cytoplasmic diffusion coefficient D_{cyt} for the tracer and the radial dimension of the fiber cells d_{fiber} (~3 μm), it is possible to

estimate the junctional permeability P_j from the effective diffusion coefficient D_{eff} as

$$P_j = \frac{D_{eff} D_{cyt}}{d_{fiber}(D_{cyt} - D_{eff})} \quad \text{(Eq. 10)}$$

Tracer Diffusion in Isolated Fiber Cells

For most of the intracellular dye diffusion experiments, the patch pipette was sealed to one end of a single fiber cell (at $x = 0$). Assuming that the dye concentration in the pipette stays constant at C_{Pip} leads to the boundary condition (equivalent to a surface evaporation condition)

$$-D_{cyt}\frac{\partial C(x,t)}{\partial t} = \alpha(C_{Pip} - C(0,t)) \quad \text{(Eq. 11)}$$

The solution for one-dimensional diffusion into a semi-infinite medium is given as (Crank, 1975)

$$C(x,t) = C_{Pip}\,\mathrm{erfc}\left(\frac{x}{2\sqrt{D_{cyt}t}}\right) - e^{\frac{\alpha}{D_{cyt}}x+\left(\frac{\alpha}{D_{cyt}}\right)^2 D_{cyt}t}\,\mathrm{erfc}\left(\frac{x}{2\sqrt{D_{cyt}t}} + \frac{\alpha}{D_{cyt}}\sqrt{D_{cyt}t}\right) \quad \begin{vmatrix} t > 0 \\ x > 0 \end{vmatrix}, \quad \text{(Eq. 12)}$$

where α is a proportionality constant which has the units of a permeability coefficient.

We can obtain the solution for the finite length fiber cell by reflection at the boundaries at $x = 0$ and $x = l$, is the length of the fiber cell (Eq. 13)

$$C(x,t) = \sum_{n=0}^{\infty} C_{Pip}\,\mathrm{erfc}\left(\frac{|2nl - |x-a||}{2\sqrt{D_{cyt}t}}\right) - e^{\frac{\alpha}{D_{cyt}}|2nl-|x-a||+\left(\frac{\alpha}{D_{cyt}}\right)^2 D_{cyt}t}\,\mathrm{erfc}\left(\frac{|2nl - |x-a||}{2\sqrt{D_{cyt}t}} + \frac{\alpha}{D_{cyt}}\sqrt{D_{cyt}t}\right) \quad \begin{vmatrix} t > 0 \\ 0 < x < l \end{vmatrix} \quad \text{(Eq. 13)}$$

Here a is the distance of the injection point from the left boundary of the fiber cell at $x = 0$. For small t this series usually converges for $n \sim 5$.

Results

Dye Diffusion in the Lens Cortex

We have loaded rhodamine-dextran and Lucifer yellow into cortical fiber cells by the mechanical damage caused by the removal of the lens capsule. We have used the gap junction impermeable tracer rhodamine-dextran to identify the point of entry for both dyes, whereas the low molecular weight Lucifer yellow was used as a tracer for gap junction mediated diffusion. The lenses were incubated in the dye solutions for 5–30 minutes and subsequently processed for examination by confocal microscopy. Since we were interested only in radial diffusion, we exclusively used equatorial sections for the assessment of dye loading and movement.

As expected, intracellular rhodamine-dextran was predominantly localized at the edge of the section consistent with the loading of damaged cells from the periphery (Fig. 2*A*). Occasionally, rhodamine-dextran fluorescence was also observed in cells at some distance from the edge of the section, and they were surrounded by nondamaged fiber cells. This loading pattern is consistent with dye entry through lesions closer to the lens poles and cytoplasmic diffusion of dye along the fiber cell. Lens sections with this "double" loading pattern were excluded from the analysis.

Extracellular rhodamine-dextran fluorescence was regularly observed and can be detected up to a depth of approximately 300 μm into the lens. This is consistent with previous reports, which documented tracer diffusion in the extracellular space between the fiber cells from the aqueous humor (Rae & Stacey, 1979).

Unlike rhodamine-dextran, Lucifer yellow fluorescence was not restricted to the damaged cells but exhibited radial diffusion away from the peripheral loading zone (Fig. 2*B*). While we occasionally observed dye diffusion along distinct columns of fiber cells, more commonly Lucifer yellow was smoothly distributed and the intensity attenuated gradually towards the lens center. The intense cytoplasmic fluorescence obscured the presence of Lucifer yellow in the extracellular space. Nevertheless, extracellular labeling was present and can be observed when lenses are incubated in dye solutions without decapsulation (*data not shown*). Lucifer yellow fluorescence levels of extracellular labeling were generally low and negligible compared to the overall fluorescence in intracellularly labeled lens sections.

Quantification of Dye Diffusion

To facilitate quantitative comparison between individual lenses, dye intensity profiles were taken exclusively from equatorial sections. Since the width of the confocal pinhole determines the depth of the focal plane and the degree of out-of-focus light entering the detector, the size of the pinhole was held constant. A pinhole of 60, which is equivalent to a focal depth of 3 μm, was chosen as optimal, and used in all experiments. Intensity profiles were always taken through the center of a column of fiber cells to minimize the contribution of extracellular labeling (Fig. 2*A* and *B*). We then plotted the intensity profiles against the radial distance from the outer boundary (Fig. 2*C*). Rhodamine-dextran intensity profiles exhibited a sharp dropoff in dye intensity, while Lucifer yellow profiles characteristically displayed an initial extended shoulder of dye intensity, which then gradually fell off towards the center of the section. The inner boundary of the dye-loading zone was determined from the rhodamine-dextran images and used to estimate the width of the loading zone for the Lucifer yellow intensity profiles.

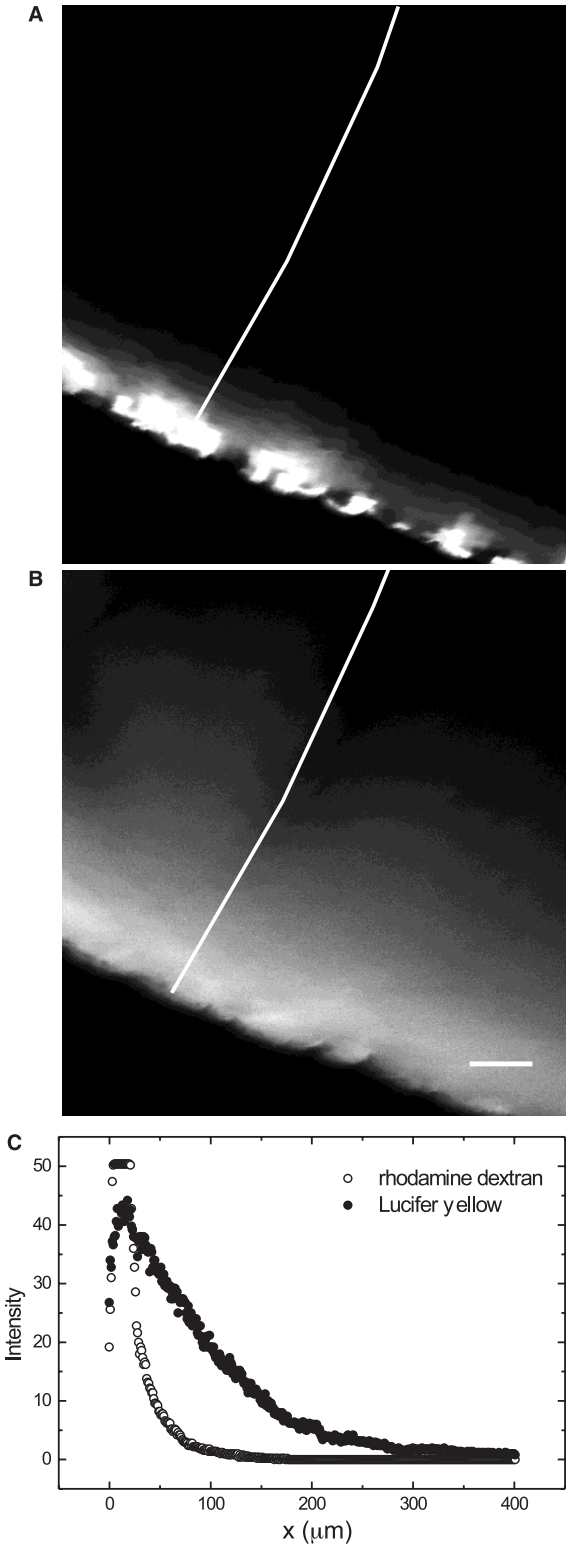

Fig. 2. Dye transfer in the lens cortex. Paired rhodamine-dextran (*A*) and Lucifer yellow (*B*) images of an equatorial section through the cortex of a decapsulated lens incubated in dye loading solution (Ca^{2+}/Mg^{2+} free PBS) for 10 min (scale bar = 50 μm). Intensity profiles were taken along a line through the center of a column of fiber cells (diagonal line) and plotted against the radial distance from the lens periphery (*C*).

For comparison between different preparations, we normalized profiles to their maximal intensity. The normalization procedure removes variations in the absolute magnitude of Lucifer yellow dye intensity between experiments, which occur due to differences in dye loading, section thickness and laser output voltage. However, in images with low intensity, this also amplifies the contribution of background fluorescence. While we tried to exclude such images from the analysis, this was not always practicable. This background fluorescence was accounted for either by background subtraction, or by introducing a constant offset term into the formulae used for curve fitting.

The resulting profiles principally fall into two categories corresponding to the two diffusion models outlined in the theory section. The profile shown in Fig. 3*A* decreases quasi exponentially and closely resembles the predicted distribution for the continuous loading model (Fig. 3*B*). In two thirds of cases, we observed another class of profiles, which is exemplified in Fig. 3*C*. These profiles are characterized by their distinctly sigmoidal shape as predicted by the bolus loading model. Note, that in the model simulation (Fig. 3*D*), the maximum intensity after 10 min is markedly decreased compared to the initial distribution. While the initial dye distribution should be roughly corresponding to the rhodamine dextran distribution, this relationship is distorted by the normalization of the Lucifer yellow profile in Fig. 3*C*.

These profiles have an interesting implication. We have to assume that once the cells were loaded with dye, their membranes either resealed or their gap junctions closed. We usually decided which model was applicable by visual inspection.

Tracer Diffusion in Isolated Fiber Cells

To calculate the gap junctional permeability of fiber cell membranes from the effective diffusion coefficients, the cytoplasmic diffusion coefficient within the fiber cells is required. To achieve this we measured cytoplasmic diffusion along the length of isolated fiber cell bundles. The dye was perfused into a single cell of a bundle via a patch pipette in the whole-cell configuration (Fig. 4). Lateral dye spreading into neighboring cells was minimized by blocking gap junction channels with halothane.

The profile shown in Fig. 4*C* was taken 140 sec after the start of intracellular perfusion along the broken line indicated in Fig. 4*B*. This rather long fiber cell bundle ($l > 500$ μm) was perfused approximately from the midpoint and allowed the observation of dye movement over long diffusion distances. The marked dropoff in intensity in the region of the pipette tip is an artefact commonly observed in these profiles. It is probably caused by absorption or scattering of fluorescent light by the glass of the pipette tip. We then applied nonlinear curve

fitting to fit. Eq. 13 to line profiles. Only single profiles at the end of the time sequence were used as the evaluation of the summation in Eq. 13 proved to be computationally very expensive. Fitting of a single line profile of about 40 points took on average about 7 min computation time on an IBM-PC equipped with a 100 MHz Pentium processor.

An example of the resulting fit is shown in Fig. 5*A*. This profile was fitted with a diffusion coefficient $D_{cyt} = (0.61 \pm 0.06) \times 10^{-6}$ cm^2/sec and a "permeability" of the pipette tip of $\alpha = (28 \pm 1) \times 10^{-6}$ cm/sec. While it was not practicable to fit the whole time series, the parameter sets obtained from this profile adequately describe the measured sequence as is shown in Fig. 5*B* and *C*, where the lower panel shows a model simulation of a time series with the parameters estimated from the fit. The average cytoplasmic diffusion coefficient was $D_{cyt} = (0.7 \pm 0.6) \times 10^{-6}$ cm^2/sec ($n = 13$).

Gap Junctional Dye Permeability in Cortical Fiber Cells

From the analysis of 21 lenses we can estimate the average effective diffusion coefficient for Lucifer yellow in the rat lens cortex $D_{eff} = (10 \pm 14) \times 10^{-8}$ cm^2/sec ($n = 21$). With an average radial width of 3–4 μm for cortical fiber cells this translates into a gap junctional permeability $P_j = (31 \pm 27) \times 10^{-5}$ cm/sec.

To further test the assumption of gap junction mediated tracer transfer and to estimate the range of modulation, we used halothane to block gap junctional communication in the lens cortex. These results are summarized in Fig. 6. As can be seen in Fig. 6*G–H*, radial intercellular diffusion of Lucifer yellow is significantly reduced following exposure of the lenses to halothane as compared to control conditions (Fig. 6*A–C*). Halothane reduced the junctional permeability by almost a factor of ten from 31×10^{-5} cm/sec to $(4 \pm 3) \times 10^{-5}$ ($n = 8$). Intracellular acidification with CO_2 also inhibits Lucifer yellow spreading albeit to a lesser extent with a junctional permeability of $(8 \pm 3) \times 10^{-5}$ cm/sec. The results are summarized in the Table. The estimated Lucifer yel-

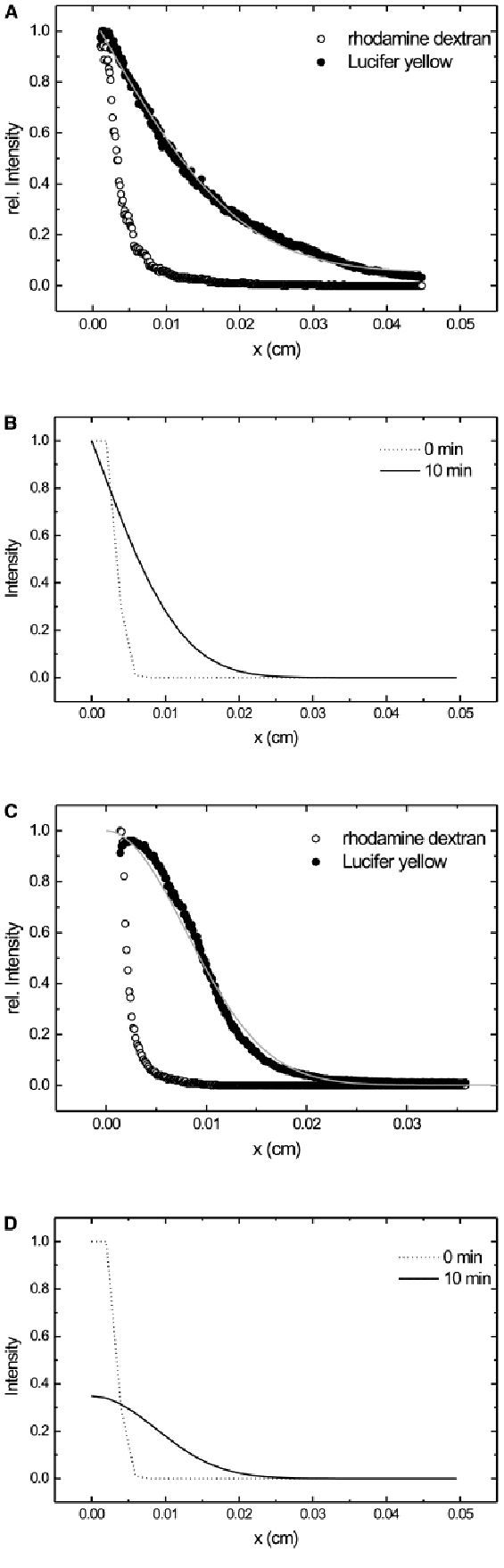

Fig. 3. Analysis of radial diffusion profiles in whole lens sections. Two classes of profiles corresponding to two diffusion models were observed. The profile shown in (*A*) decreases quasi exponentially and closely resembles the predicted distribution for the continuous loading model (*B*). More prominently, we observed profiles with the distinctly sigmoidal shape (*C*) predicted by the bolus loading model (*D*). The intensity profile given in (*A*) was best fitted with Eq. 5, with $D_{eff} = (10.3 \pm 0.5) \times 10^{-8}$ cm^2/sec ($t_d = 20$ min). The profile (*C*) was fitted with Eq. 6, with $D_{eff} = (5.1 \pm 0.2) \times 10^{-8}$ cm^2/sec ($t_d = 10$ min). The width of the loading zone was taken as the width of the rhodamine dextran intensity profile and was fixed to $h = 23$ μm.

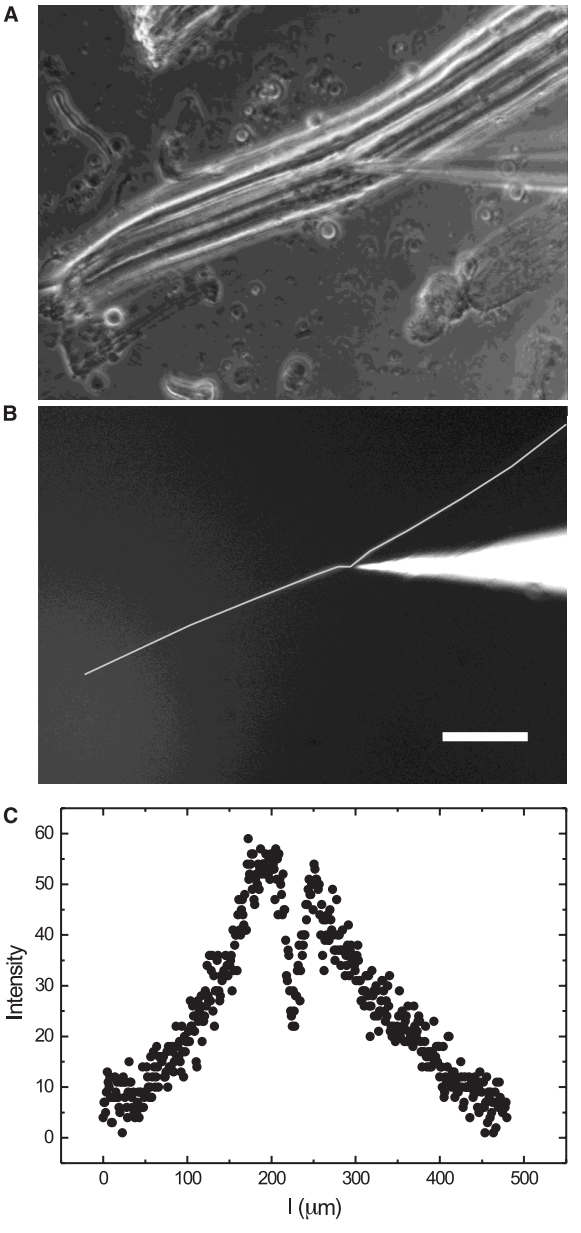

Fig. 4. Intracellular dye diffusion in isolated lens bundles. Phase contrast (*A*) and epifluorescence image (*B*) of an isolated lens fiber cell bundle perfused with Lucifer yellow for 140 sec (scale bar = 100 μm). (*C*) Intensity profile taken along the length of the fiber cell (dotted line in panel (*B*)). The origin ($l = 0$) is the lower left end of the fiber cell. The dropoff in intensity at about the midpoint is an artefact caused by absorption or scattering of fluorescent light by the pipette tip.

low permeabilities for halothane and CO_2-treated lenses were compared to control lenses by 1-way ANOVA assuming a lognormal distribution. Using a 5% error criterion ($P \leq 0.05$), halothane and CO_2-treated lenses had significantly lower permeability as compared to control lenses confirming that dye diffusion is mediated by gap junctions.

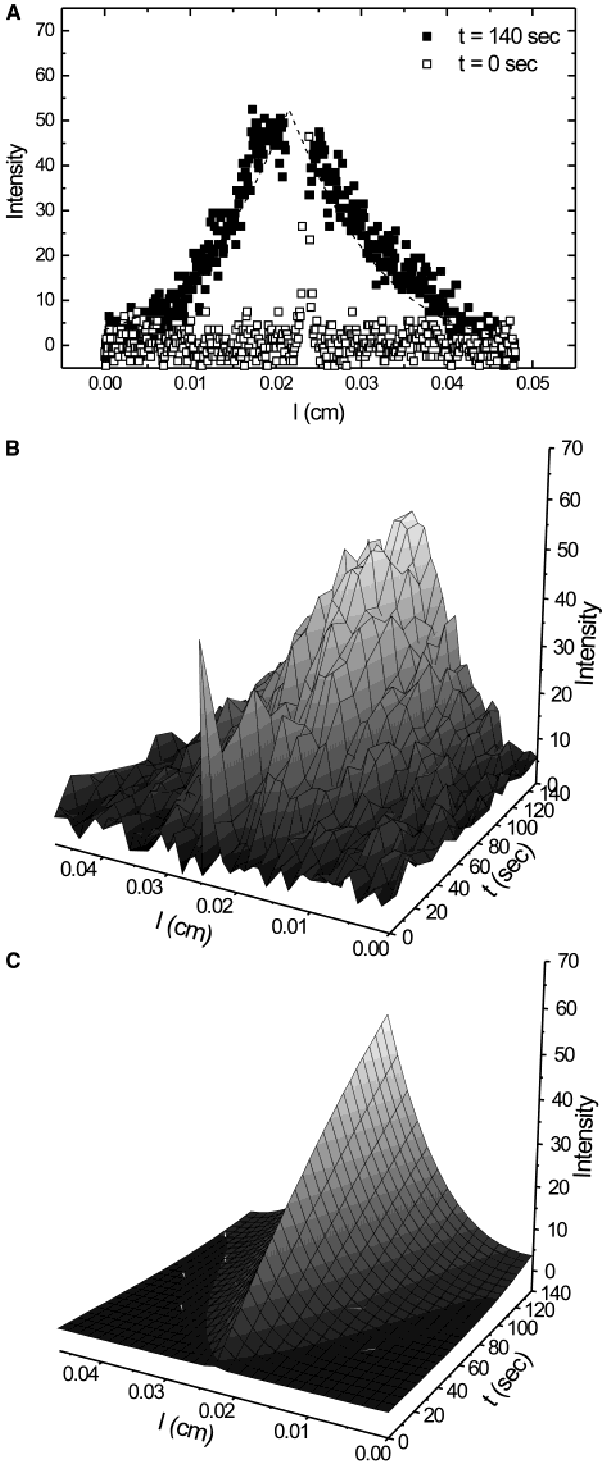

Fig. 5. Analysis of diffusion profiles in isolated fiber cells. The intensity profile given in Fig. 4*C* was fitted with Eq. 13. The resulting parameters were $D_{cyt} = (0.61 \pm 0.06) \times 10^{-6}$ cm^2/sec, and $\alpha = (28 \pm 1) \times 10^{-6}$ cm/sec. The diffusion time ($t_d = 140$ sec), intensity at the pipette tip ($I_{Pip} = C_{Pip} = 160$), fiber cell length ($l = 0.048$ cm), and displacement of the pipette tip ($a = 0.0223$ cm) were taken by direct measurement from the image and held fixed for the fit. The resulting parameter estimates were then used to simulate the time evolution of the dye intensity. As can be seen in the lower two panels, the measured time sequence (*B*) is in good agreement with the simulated data (*C*) for the given parameter set.

Discussion

We have developed a simple method, which allows us to quantify intercellular dye diffusion through gap junctions in the mammalian lens. This method takes advantage of the quasi-spherical geometry of the lens, the highly ordered arrangement of the lens fiber cells into concentric membrane layers, and the abundance of gap junctions that link the cells with each other. These properties greatly simplify the models employed in estimating the effective dye diffusion coefficient. The exceptional length of the fiber cells and the availability of isolation protocols also allow us to measure the cytoplasmic diffusion coefficient of a dye independent of the intercellular diffusion. These quantities can then be used to determine the (absolute) gap junctional permeability of fiber cell membranes, which, similar to the electrical conductance of gap junctions, is a quantity that is comparable between preparations.

Model Assumptions and Limitations for the Analysis

For the derivation of the analytical formulae for radial tracer distribution in the lens, we have made a number of critical assumptions that may affect the accuracy of our estimates. First, we have assumed that the lens is a sphere rather than a lentoid. In this study we used isolated lenses from juvenile rats, which are very close to spherical. We have further assumed, that the diameter of the lens is large compared to the diffusion distance from the periphery. This allows us to ignore the correction term for spherical diffusion in the diffusion equation and to use a linear model instead. We have validated this assumption with model simulations for a lens with 4 mm diameter and confirmed that there is virtually no difference between the profiles for the spherical versus the linear model.

A further assumption related to this is, that the boundary conditions at the lens surface are homogeneous

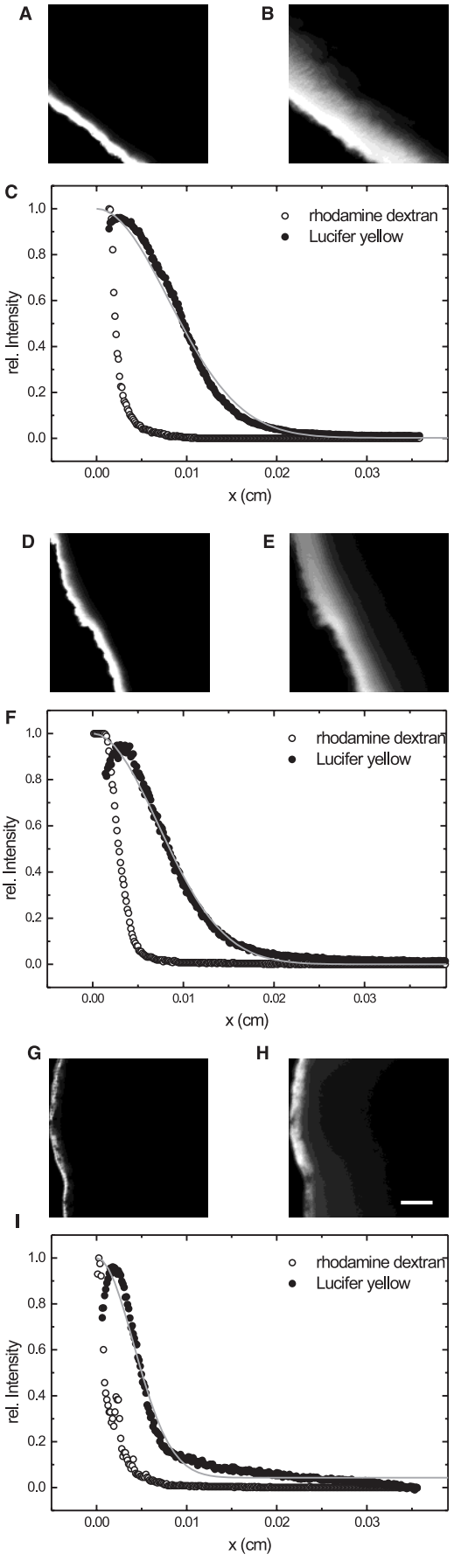

Fig. 6. Modulation of Lucifer yellow permeability by intracellular acidification and halothane. Paired rhodamine-dextran (*A,D,G*) and Lucifer yellow (*B,E,H*) images of equatorial cortical sections from decapsulated lenses incubated in: control (*A–C*), CO_2 saturated (*D–F*), and halothane saturated bath solution. (G-I) Confocal images used identical confocal pinhole and PMT settings (scale bar = 100 μm). Radial intercellular diffusion of Lucifer yellow is partially inhibited by acidification with 100% CO_2 as compared to control conditions while incubation with halothane significantly blocks dye spreading into the lens cortex. The effective diffusion coefficients estimated by fitting Eq. 6 to the profiles were: $D_{eff} = (5.1 \pm 0.2) \times 10^{-8}$ cm^2/sec for the control lens, and $D_{eff} = (3.9 \pm 0.2) \times 10^{-8}$ cm^2/sec, and $D_{eff} = (1.3 \pm 0.1) \times 10^{-8}$ cm^2/sec for CO_2 (*F*) and halothane (*I*) treated lenses, respectively.

Table. Diffusion constants in lens cortex

	Control	Low pH	Halothane
D_{eff} (cm^2/sec)	$(10 \pm 14) \times 10^{-8}$	$(3 \pm 2) \times 10^{-8}$	$(2 \pm 2) \times 10^{-8}$
P_j (cm/sec)	$(31 \pm 27) \times 10^{-5}$	$(8 \pm 3) \times 10^{-5}$	$(4 \pm 3) \times 10^{-5}$
n	21	8	8

throughout the whole surface area and in time. This means, that dye concentration and dye uptake is the same everywhere on the lens surface. The first condition is met by the homogeneous concentration of dye in the loading solution. However, we have observed regions where the intensity profiles follow the continuous loading model and regions that follow the bolus loading model in the same lens section. There is even the possibility that some regions of the lens may initially be loaded continuously and then reseal and thus follow a bolus model. The actual intensity profiles are therefore most likely a mixture between both models with some bias towards either of the two ideal cases. While this distinction is of some importance for mechanistic considerations on dye loading, in practice the diffusion coefficients estimated by fitting either of the two models were not too different considering the precision of the fitting procedure.

We have also ignored convective transport in angular direction through the cytoplasm of the fiber cells. This transport mechanism was proposed by a model for lens transport (Mathias et al., 1985, 1997) and has recently been implicated by tracer injection studies *in situ* in the lens (Rae et al., 1996). However, the effects of angular transport on dye diffusion should be minimal in the equatorial plane of the lens, which is why we have restricted our analysis to equatorial sections. A further assumption is that after dye loading there is no significant loss of dye through the cell membranes. We have confirmed this by incubation of whole nondecapsulated lenses in dye loading solutions. Under these conditions, we only observed extracellular staining indicating that in the absence of damage the fiber cell membranes are impermeable to the dyes used in this study. Similar results have been reported previously for Procion yellow in isolated whole lenses (Rae & Stacey, 1979).

The most critical assumption, however, is that the effective diffusion coefficient within the lens is uniform. This implies that the radial and angular distribution of gap junctions must be homogeneous throughout the lens. This clearly is a simplification of the real situation, as it is known that the number and size of gap junctions in the cortex changes in both angular and radial directions (Gruijters, Kistler & Bullivant, 1987). In some cases we have observed intensity profiles with marked kinks or bends at about 150 μm radial distance. This feature could be reproduced in model simulations, if we assumed that there was either a local discontinuity of the diffusion coefficient (that is only one cell layer thick) or that there was a boundary between two compartments with different diffusion coefficients. Since the density of gap junction plaques decreases in the angular direction from equator to the lens poles we would also expect a decrease in junctional permeabilities at the poles vs. the equator. Cytoplasmic diffusion along the length of a fiber cell may partially compensate for this and, therefore, the effective diffusion coefficient D_{eff} calculated from intensity profiles of equatorial sections estimates a weighted average between the (larger) junctional permeabilities at the equator and the (smaller) permeabilities at the poles. For this problem, there is no analytical solution to the diffusion equation and we would have to fit the intensity profiles with the diffusion equations directly, which is beyond the scope of this current presentation. Variable diffusion coefficients would introduce a number of additional free parameters into the fitting model, which could render the interpretation of the results ambiguous. Ultimately it would be desirable to analyze the dye distribution in whole axial sections rather than equatorial (cross) sections. This would enable us to accommodate such factors as angular transport and inhomogeneous diffusion coefficients into a more detailed analysis of lens transport properties. Despite these cautions, we believe that our present analysis represents a valid first approximation to modeling gap junction permeability in the lens cortex and that it provides a good representation within the limits of measurements possible in biological specimens.

Tracer Diffusion in Isolated Fiber Cells

The cytoplasmic diffusion coefficient is a critical parameter for the calculation of gap junctional permeabilities from gross diffusion profiles. However, to obtain cytoplasmic diffusion coefficients long diffusion distances are required, which are usually not available in normal cell preparations. The lens has considerable advantages in this respect due to the long and regular shape of the lens fiber cells. The septate axon of the earthworm is another cell type, which is sufficiently long to allow these measurements (Brink & Ramanan, 1985; Ramanan & Brink, 1990). In these cells a cytoplasmic diffusion coefficient of 2×10^{-6} cm^2/sec was determined for Lucifer yellow, which compares well to the value of 0.6×10^{-6} cm^2/sec we have obtained in lens fiber cells. The slightly lower diffusion coefficient in fiber cells may be attributed to the unusually high protein content (crystallins) of the fiber cells.

Gap Junctional Dye Permeability in Cortical Fiber Cells

Due to its unique properties and its dependence on gap junctional transport, the lens has attracted a number of

investigations into tracer diffusion between cells of the lens (Goodenough, Dick II & Lyons, 1980; Schuetze & Goodenough, 1982; Miller, Zampighi & Hall, 1992; Miller, 1995; Bassnett et al., 1994; Prescott et al., 1994; Rae et al., 1996). While Rae and coworkers (Rae et al., 1996) have reported a junctional permeability of $P_j^{e-f} = (4.4 \pm 3.5) \times 10^{-6}$ cm/sec for epithelial-fiber cell junctions in the rat lens, ours is the first study to specifically measure fiber-fiber junctional permeabilities. Our value for the fiber-fiber permeability of P_j^{f-f} of $(31 \pm 27) \times 10^{-5}$ cm/sec is significantly higher than the value that Rae et al. (1996) reported for epithelial-fiber cell junctions. This is to be expected since fiber cells in the outer cortex are linked by a large number of gap junction plaques (Gruijters et al., 1987; Goodenough, 1992). In contrast the paucity of gap junction structures between epithelial and fiber cells (Bassnett et al., 1994; Prescott et al., 1994) suggests a substantially lower permeability for this interface. Rae et al. (1996) also report a fiber-fiber permeability of P_j^{f-f} of 2.8×10^{-6} cm/sec estimated from a single measurement in the polar region of a fiber cell. However, given the assumptions made in this estimation and the uncertainties of a single measurement, the variability may be quite large. When compared with gap junctional conductances obtained from impedance analysis of the frog lens this value appears to be at least one order of magnitude too small while the fiber-fiber permeability reported here is in reasonable agreement with both the electrical data and the abundance of gap junction structures in fiber cells.

In summary we have used a simple method to introduce tracer dyes into the lens and have developed the theoretical framework to quantify gap junctional permeability. Gap junctions are widely acknowledged as essential for the maintenance of lens transparency and abnormal gap junction closure has been proposed to be involved in diabetic cataractogenesis (Kistler et al., 1999). The techniques outlined in this report should now enable us to detect and quantify changes in gap junction permeability during early cataractogenesis.

The authors are grateful to Dr. Colin Green for technical assistance and helpful discussion with confocal microscopy. We would also like to thank Drs. Christian Soeller and Mark Tunstall for their helpful discussions during the preparation of this manuscript. This work was funded by The Auckland Medical Research Foundation, the New Zealand Lottery Grants Board, the Health Research Council of New Zealand, and the Marsden Fund.

References

Bassnett, S., Kuszak, J.R., Reinisch, L., Brown, H.G., Beebe, D.C. 1994. Intercellular communication between epithelial and fiber cells of the eye lens. *J. Cell Sci.* **107:**799–811

Brink, P.R. 1996. Gap junction channel gating and permselectivity—Their roles in coordinated tissue function. *Clin. Exp. Pharm. Physiol.* **23:**1041–1046

Brink, P.R., Ramanan, S.V. 1985. A model for the diffusion of fluorescent probes in the septate giant axon of earthworm — axoplasmic diffusion and junctional membrane permeability. *Biophys. J.* **48:**299–309

Crank, J. 1975. The Mathematics of Diffusion. Oxford University Press, Oxford

Donaldson, P.J., Dong, Y., Roos, M., Green, C., Goodenough, D.A., Kistler, J. 1995. Changes in lens connexin expression lead to increased gap junctional voltage dependence and conductance. *Am. J. Physiol.* **269:**C590–C600

Eckert, R., Donaldson, P., Kistler, J. 1998. A distinct membrane current in rat lens fiber cells isolated under calcium free conditions. *Invest. Ophthalmol. Vis. Sci.* **39:**1280–1285

Elfgang, C., Eckert, R., Lichtenberg-Fraté, H., Butterweck, A., Traub, O., Klein, R.A., Hülser, D.F., Willecke, K. 1995. Specific permeability and selective formation of gap junction channels in connexin-transfected HeLa cells. *J. Cell Biol.* **129:**805–817

el-Fouly, M.H., Trosko, J.E., Chang, C.-C. 1987. Scrape-loading and dye transfer—a rapid and simple technique to study gap junctional intercellular communication. *Exp. Cell Res.* **168:**422–430

Flagg-Newton, J., Simpson, I., Loewenstein, W.R. 1979. Permeability of the cell-to-cell membrane channels in mammalian cell junction. *Science* **205:**404–407

Gong, X.H., Li, E., Klier, G., Huang, Q.L., Wu, Y., Lei, H., Kumar, N.M., Horwitz, J., Gilula, N.B. 1997. Disruption of α_3 connexin gene leads to proteolysis and cataractogenesis in mice. *Cell* **91:**833–843

Goodenough, D.A. 1992. The crystalline lens. A system networked by gap junctional intercellular communication. *Sem. Cell Biol.* **3:**49–58

Goodenough, D.A., Dick II, J.S.B., Lyons, J.E. 1980. Lens metabolic cooperation: a study of mouse lens transport and permeability visualized with freeze-substitution autoradiography and electron microscopy. *J. Cell Biol.* **86:**576–589

Gruijters, W.T.M., Kistler, J., Bullivant, S. 1987. Formation, distribution and dissociation of intercellular junctions in the lens. *J. Cell Sci.* **88:**351–359

Kistler, J., Christie, D., Bullivant, S. 1988. Homologies between gap junction proteins in lens, heart and liver. *Nature* **331:**721–723

Kistler, J., Lin, J.S., Bond, J., Green, C., Eckert, R., Merriman, R., Tunstall, M., Donaldson, P. 1998. Connexins in the lens: are they to blame in diabetic cataractogenesis? *In:* Novartis Foundation Symposium 219—Gap junction-mediated intercellular signaling in health and disease. pp. 97–112. Wiley, London

Loewenstein, W.R. 1981. Junctional intercellular communication: the cell-to-cell membrane channel. *Physiol. Rev.* **61:**829–913

Mathias, R., Rae, J.L., Ebihara, L., McCarthy, R.T. 1985. The localization of transport properties in frog lens. *Biophys. J.* **48:**423–434

Mathias, R.T., Rae, J.L., Baldo, G.J. 1997. Physiological properties of the normal lens. *Physiol. Rev.* **77:**21–50

Miller, A. 1995. Quantitative junctional permeability measurements using the confocal microscope. *Microsc. Res. Tech.* **31:**387–395

Miller, A.G., Zampighi, G.A., Hall, J.E. 1992. Single-membrane and cell-to-cell permeability properties of dissociated embryonic chick lens cells. *J. Membrane Biol.* **128:**91–102

Neyton, J., Trautmann, A. 1985. Single-channel currents of an intercellular junction. *Nature* **317:**331–335

Paul, D.L., Ebihara, L., Takemoto, L.J., Swenson, K.I., Goodenough, D.A. 1991. Connexin46, a novel lens gap junction protein, induces voltage-gated currents in nonjunctional plasma membrane of *Xenopus* oocytes. *J. Cell Biol.* **115:**1077–89

Prescott, A., Duncan, G., van Marle, J., Vrensen, G. 1994. A correlated study of metabolic cell communication and gap junction distribution in the adult frog lens. *Exp. Eye Res.* **58:**737–746

Press, W.H., Teukolsky, S.A., Vetterling, W.T., Flannery, B.P. 1992. Numerical Recipes in C-The Art of Scientific Computing. Cambridge University Press, Cambridge

Rae, J.L., Bartling, C., Rae, J., Mathias, R.T. 1996. Dye transfer between cells of the lens. *J. Membrane Biol.* **150:**89–103

Rae, J.L., Stacey, T. 1979. Lanthanum and Procion yellow as extracellular markers in the crystalline lens of the rat. *Exp. Eye Res.* **28:**1–21

Rafferty, N.S. 1985. Lens morphology. *In:* The ocular lens–structure, function, and pathology. H. Maisel, editor. pp. 1–60. Marcel Dekker, New York

Ramanan, S.V., Brink, P.R. 1990. Exact solution of a model of diffusion in an infinite chain or monolayer of cells coupled by gap junctions. *Biophys. J.* **58:**631–639

Schuetze, S.M., Goodenough, D.A. 1982. Dye transfer between cells of the embryonic chick lens become less sensitive to CO_2 treatment with development. *J. Cell Biol.* **92:**694–705

Taylor, D.L., Salmon, E.D. 1989. Basic fluorescence microscopy. *Meth. Cell Biol.* **29:**207–237

Veenstra, R.D. 1996. Size and selectivity of gap junction channels formed from different connexins. *J. Bioenerget. Biomembr.* **28:**327–337

Veenstra, R.D., DeHaan, R.L. 1986. Measurement of single channel currents from cardiac gap junctions. *Science* **233:**972–974

Werner, R. 1998. Gap Junctions — Proceedings of the 8th International Gap Junction Conference Key Largo, Florida. pp. 385. IOS Press, Amsterdam

White, T.W., Bruzzone, R., Goodenough, D.A., Paul, D.L. 1992. Mouse C×50, a functional member of the connexin family of gap junction proteins, is the lens fiber protein MP70. *Mol. Biol. Cell* **3:**711–20

White, T.W., Goodenough, D.A., Paul, D.L. 1998. Targeted ablation of connexin50 in mice results in microphthalmia and zonular pulverulent cataracts. *J. Cell Biol.* **143:**815–825

Appendix

Modeling of Diffusion Profiles in the Lens

Another possible approach to modeling diffusion processes is the numerical solution of the underlying partial differential equations. For time-dependent (initial value) problems, this usually involves the numerical solution of linear difference equations. Numerical solutions have the additional advantage, that it is relatively straightforward to include options such as local variations in the diffusion coefficient, binding, or convective transport processes.

For the derivation of the linear difference equations, we start with the radial diffusion equation

$$\frac{\partial C}{\partial t} = D\left(\frac{\partial^2 C}{\partial r^2} + \frac{2}{r}\frac{\partial C}{\partial_r}\right),$$

This translates into the following explicit (FTCS) linear difference equation

$$\frac{C(r_i,t_{j+1}) - C(r_i,t_j)}{\Delta t} = D\left(\frac{C(r_{i+1},t_j) - 2C(r_i,t_j) + C(r_{i-1},t_j)}{\Delta r^2} + \frac{2}{r}\frac{C(r_{i-1},t_j) - C(r_{i+1},t_j)}{2\Delta r}\right)$$

For constant D, and

$$\frac{C(r_i,t_{i+1}) - C(r_i,t_j)}{\Delta t} = \frac{D(r_{i+1/2})C(r_{i+1},t_j) - D(r_{i+1/2})C(r_i,t_j) - D(r_{i-1/2})C(r_i,t_j) + D(r_{i-1/2})C(r_{i-1},t_j)}{\Delta r^2} + \frac{2}{r}\frac{D(r_{i-1/2})C(r_{i-1},t_i) - D(r_{i+1/2})C(r_{i+1},t_j)}{2\Delta r}$$

for spatial variations of D (Press et al., 1992). Here,

$$r_i = r_0 + i\Delta r \quad |i = 0,1,2,\ldots$$

$$t_j = t_0 + j\Delta t \quad |j = 0,1,2,\ldots$$

$$D(r_{i+1/2}) = \frac{D(r_i) + D(r_{i+1})}{2}$$

are the discretized radial and time coordinates and the local diffusion coefficient between radial grid lines, respectively. By solving for $C(r_i,t_{j+1})$ we obtain the following recursive formula

$$C(r_i,t_{j+1}) = C(r_i,t_j) + \Delta t D\left(\frac{C(r_{i+1},t_j) - 2C(r_i,t_j) + C(r_{i-1},t_j)}{\Delta r^2} + \frac{2}{r}\frac{C(r_{i+1},t_j) - C(r_{i+1},t_j)}{2\Delta r}\right),$$

which describes the evolution of the radial tracer distribution in time from a given initial distribution $C_0(r)$. The two cases of dye loading discussed for the analytical solutions can be obtained by applying the appropriate boundary conditions at $r = 0$ and $r = R$, as given above.

The explicit linear difference equations are numerically stable only for small values of Δt ($\Delta t \leq (\Delta x)^2/2D$) and, therefore, only efficient for small diffusion times. However, since for most experiments the diffusion times are relatively short (5–15 min), we feel that this method is still appropriate ($\Delta t \sim 3$ *sec*).